

Multifragmentation of charge asymmetric nuclear systems.

A.B. Larionov^{1,2}, A.S. Botvina^{3,4}, M. Colonna⁵, M. Di Toro⁵

¹ *Institut für Theoretische Physik, Universität Giessen, D-35392 Giessen, Germany*

² *Russian Research Center "I.V. Kurchatov Institute", 123182 Moscow, Russia*

³ *INFN and Dipartimento di Fisica, Bologna, Italy*

⁴ *Institute for Nuclear Research, Russian Academy of Science, 117312 Moscow, Russia*

⁵ *Laboratori Nazionali del Sud, Via S. Sofia 44, I-95123 Catania, Italy*

and University of Catania

Abstract

The multifragmentation of excited spherical nuclear sources with various N/Z ratios and fixed mass number is studied within dynamical and statistical models. The dynamical model treats the multifragmentation process as a final stage of the growth of density fluctuations in unstable expanding nuclear matter. The statistical model makes a choice of the final multifragment configuration according to its statistical weight at a global thermal equilibrium. Similarities and differences in the predictions of the two models on the isotopic composition of the produced fragments are presented and the most sensitive observable characteristics are discussed.

PACS numbers: 25.70.Pq, 21.65.+f, 24.10.Cn, 24.10.Pa, 24.60.Ky

I. INTRODUCTION

In recent years two main models, statistical and dynamical, have been suggested to describe nuclear multifragmentation, i.e. the production of several intermediate mass fragments in heavy ion collisions. In the statistical picture a global equilibrium is assumed in a freeze out volume and the various break-up channels are selected in a microcanonical way according to the statistical weight of the corresponding partition, given by the channel entropy [1,2]. In the dynamical model clusters are directly formed during the expansion phase by a collective response of the interacting nuclear matter in low density unstable regions, the spinodal decomposition mechanism [3,4].

The standard applicability condition of a statistical approach in nuclear reactions is a dominance of the available phase space over transition matrix elements. Usually this will require a lot of interactions between nucleons and a related characteristic time scale which can be considerably larger than the time of the growth of mean field instabilities in the dynamical approach. Therefore one would expect a corresponding validity for quite different physical scenarios of formation of the highly excited source which will fragment [see discussion in Ref. [3] and in the conclusions of Ref. [4]]. In fact the two models seem to lead to very similar predictions for charge and kinetic energy distributions of the same class of fragmentation events [5–7]. One of the aims of this paper is to suggest new observables in a study of isospin effects that should help to disentangle between the two pictures.

Moreover the effect of charge asymmetry on fragment production is of large theoretical [8–15] and experimental [16–22] interest. One important reason is that it could be related to the fundamental problem of extracting information on the nuclear equation of state (EOS), in particular on the symmetry energy, at subnuclear densities.

In this work, on the basis of both statistical and dynamical models, we study the multifragmentation process in highly excited heavy nuclei. Such systems can be created in central collisions of two heavy ions at intermediate energies ($E_{lab} \sim 100$ MeV/nucleon) or in reactions induced by high energy ($E_{lab} \sim 1$ GeV/nucleon) light projectile on heavy target.

We present various measurable characteristics: charge yields, intermediate mass fragment $Z \geq 3$ (IMF) multiplicity distributions, N/Z ratio versus charge of fragment, isotopic ratios in order to understand their sensitivity to the neutron excess of the source nucleus.

The interplay of symmetry and Coulomb energies defines the N/Z ratio of formed fragments. Here and below, the *hot* fragments produced just after multifragment breakup are discussed, if the opposite is not indicated. In the fast spinodal decomposition process [13,14], a higher density (liquid) phase becomes isotopically more symmetric and a lower density (gaseous) phase accumulates the most part of the neutron excess of the system. This effect is related to the increase of the potential symmetry energy per nucleon with the density at subnuclear densities $\rho \leq \rho_{eq}$, $\rho_{eq} = 0.17 \text{ fm}^{-3}$, as given by all realistic effective interactions [23,24]. Therefore when the initially space-uniform low-density neutron-rich nuclear matter will clusterize the protons will be concentrated inside clusters. The fragment N/Z ratio should decrease in this case with the charge number Z , since heavy clusters are associated with the liquid phase while light ones are created in a coalescence process taking place in the gaseous phase. On the other hand the Coulomb interaction, not present in the nuclear matter analyses of ref.s [13,14] will act in the opposite direction preventing the proton clustering. Therefore it is important to work out a simulation for a realistic finite nuclear source. We will use a Stochastic Mean Field (SMF) approach [3], extension of transport nuclear models to a consistent treatment of fluctuations. We have to stress that fragments produced in the *fast* spinodal decay will be sensitive to the density dependence of the symmetry energy.

In the case of finite nuclei in the stability valley we have in fact a growth of the N/Z ratio with the charge number Z . One expects this behaviour of N/Z also for fragments which are produced in the *slow* statistical process at thermal equilibrium, since only the free energy of the system is important here, that is the sum of free energies of fragments plus the energy of the Coulomb interaction between fragments. In this case the memory of the dynamical features associated with the spinodal decay is lost, leading to a chaotic evolution, where all possible multifragmentation channels will be open [25]. In the paper we will use the Statistical Multifragmentation Model (SMM) (see Ref. [26]).

Another important discrepancy in the predictions of the two models is expected at the level of variances with respect to mean values. Indeed we would have a much narrower isotopic mass distributions in the dynamical description than in the statistical one, since the strong thermal fluctuations, inherent in the statistical approach where a wide range of channels can contribute, will not be present in the dynamical model.

These two striking discrepancies, on the background of an overall agreement in the predictions of the models on other isospin-averaged observables, will be discussed below on the basis of numerical results.

II. COMPARISON PROCEDURE: CHOICE OF THE EXCITED SOURCE

It is known from earlier studies [27], that in the mean field description a nucleus is very stable with respect to the multifragment breakup. In recent years stochastic extensions of mean-field approaches have been introduced, well suited to describe the so-called spinodal decomposition, i.e. a multifragmentation process due to the occurrence of volume instabilities [28,29]. In this picture the fragment production is due to the growth of the most important collective unstable modes. In violent reactions at intermediate energy it is possible to observe the formation of a hot and dense nuclear source, that subsequently expands and enters the unstable region of the nuclear matter phase diagram, the spinodal region. Within this scenario, because of the instability, the fluctuations of the local density are amplified, leading to a break-up of the nuclear system into many fragments. If the time scales of the expansion and of the instability growth are matching we will expect a fragmentation pattern with memory of the collective response of the unstable nuclear matter. From the above discussion it is clear that in a dynamical picture part of the initial available energy should be put in a collective radial flow.

In the following we will consider stochastic mean field (SMF) calculations. Fluctuations are introduced at the initial time by agitating randomly the density profile. The amplitude of these fluctuations is calculated according to a Boltzmann-Langevin theory and depends

on local density and temperature of the source [3].

We have performed SMF calculations (see Ref. [3]) of the multifragment break-up of $A = 197$ isobars with $Z = 95, 79$ and 63 . The temperature of the source nuclei was chosen to be $T = 3$ MeV, that is typical for multifragmentation in heavy ion collisions. A radial flow energy of 3 MeV/nucleon was added in order to prevent the resilience of the initially expanded source ($\rho_{init}^{SMF} = 0.5\rho_{eq}$) to the normal density. The total excitation energy per nucleon, which includes thermal, compressional and flow contributions was $E^*/A = 8$ MeV. The time evolution of the expanding source was followed until 150 fm/c. At this time, the fragment formation process due to the density fluctuation growth is already finished, and one can extract various characteristics of hot fragments from the phase space distribution, using a coalescence procedure, see Refs. [3,30].

We have performed 100 runs for each source nucleus. The accumulated statistics is enough to calculate the charge yields of fragments, the average N/Z ratios and their fluctuations as a function of Z (see Figs. 3,6,7).

In parallel, we have applied the SMM model [26] to the same sources taking also an overall excitation energy $E^*/A = 8$ MeV and a freeze-out volume $V_{f.o.} = 3V_0$, where $V_0 = 4\pi R_0^3/3$ is the volume of a ground state nucleus, $R_0 = 1.2A^{1/3}$. We remark that the corresponding freeze-out density $\rho_{f.o.}^{SMM} = \rho_{eq}/3$ is less than the initial density ρ_{init}^{SMF} . However, in SMF the initial source expands while fragments are forming, so when they are well defined (i.e. they do not feel anymore the nuclear interaction), the volume inside which the intermediate mass fragments are located is larger than the initial volume of the unstable source.

In Fig. 1 we show the radial distribution of the SMF-fragments at $t=150$ fm/c. The spatial ordering of fragments vs. their masses is clearly seen at $r = 7 \div 13$ fm, showing a bubble-like distribution with larger fragments placed closer to the center. Notice, that the radius of the sphere containing the farthest fragments (~ 10 fm) gives just nearly the freeze-out volume chosen for the SMM calculation. In the SMM the hot fragments are distributed more uniformly in the freeze-out volume, though a similar ordering trend is observed because of conditions of finiteness and nonoverlapping of fragments. The different space distributions

of fragments should be also reflected in a different pattern of the Coulomb acceleration, with on average a larger Coulomb interaction energy for the SMM fragments.

In Fig. 2 we present the kinetic energy of fragments as a function of Z for the SMF at $t = 150$ fm/c (dashed histogram) and after the Coulomb acceleration (full histogram), and for the SMM (stars – before Coulomb acceleration, squares – after Coulomb acceleration). The kinetic energy of heavy SMF-fragments is close to the one of the SMM-fragments before Coulomb acceleration (~ 10 MeV), which is practically independent of Z since thermalization is assumed in the statistical model. The kinetic energy of the SMF-fragments increases with Z (for $Z \leq 10$), reaches a maximum and then decreases at larger Z . This trend can be due to the Coulomb acceleration (that in the SMF calculations the fragments start to feel already before $t = 150$ fm/c) and to the presence of a radial flow, though much reduced when compared to the initial one. The decrease at larger Z is due to the preferential formation of heavy fragments closer to the center of the system (see Fig. 1). The Coulomb acceleration of the SMF-configuration increases the kinetic energies of the SMF-fragments at the final time. However the final energies are below the SMM curve after Coulomb acceleration, due to the smaller Coulomb energy stored in the bubble-like SMF-configurations.

As it was pointed out in [31] the statistical approach can be used for the description of the fragment formation process even at high energies once the preequilibrium emission leading to some mass and energy loss is taken into account. We have a similar effect in the present SMF calculations: a part of nucleons escapes from the fragment formation region fast and does not participate in the process. However this part is small in our case and does not influence the final conclusions.

In Fig. 3 the fragment charge yields are presented for both models. We see that slopes and absolute values of the charge yields for statistical and dynamical models are very similar for $Z > 5$. This is indeed a good trigger for a meaningful comparison of the fragment properties. We remark that in the spinodal decomposition mechanism the direct production of primary light clusters is reduced due to the finite range of the nuclear force which prevents the the propagation of short unstable wave lengths [3]. Moreover the study of light clusters

is out of the scope of mean-field approaches, so in the following we will concentrate on IMF ($Z \geq 3$) properties. The results for *cold* fragments (Fig.3d) have been obtained with an evaporation decay described in the next section.

The IMF yield is roughly proportional to the charge number of the fragmenting source. This can be seen from the IMF multiplicity distributions presented in Fig. 4. The effect is weaker in the SMF results. An explanation could be a very weak dependence of the wavelength of the most unstable mode on the charge asymmetry of the system (see Ref. [13,14]). In general the SMM predictions give larger yields for primary IMFs, mostly due to the enhanced yield of fragments with $Z \leq 5$ discussed above (see Fig. 3). We remind that the IMF has a charge number $Z \geq 3$ by its definition.

III. FRAGMENT PROPERTIES AND ISOTOPIC RATIOS

In order to compare the energy balance in dynamical and statistical calculations we present in Fig. 5 the excitation energies of the hot fragments. For instance, we see from Fig. 5c, that for the initial source with larger asymmetry, $Z = 63$, the primary SMM-fragments are excited stronger than the SMF-ones. This is interesting since we would expect the opposite after the discussion on kinetic energies presented in Fig. 2, since SMM-fragments have also larger kinetic energies. This is a consequence of two main effects: (i) In the dynamical evolution a large fraction of energy is dissipated in the neutron-rich gas and the primary fragments of the liquid phase are less excited; (ii) In the statistical picture an increasing share of surface contributions in light IMFs causes a slight increase of their excitation energy per nucleon. However in general the difference between the fragment excitation energies from SMF and SMM calculations is always no more than 0.5 MeV/nucleon.

A. Mean values

In Fig. 6 the average ratio $\langle N/Z \rangle$ of produced hot (a,b,c) and cold (d) fragments is shown versus the fragment charge number Z . For the almost symmetric source with $Z = 95$, (a),

fragments have practically the same initial N/Z (see arrow). For the gold fragmentation $Z = 79$, (b), the fragments have slightly lower N/Z ratio with respect to the one of the initial source due to the enhanced neutron emission during the multifragment breakup. This reduction of the N/Z of hot fragments becomes more pronounced for the mostly neutron rich source $Z = 63$, (c). In this case we observe also a clear effect of the density dependence of the symmetry energy: dynamical calculation (solid histogram) gives the decrease of the N/Z with charge number Z at $3 \leq Z \leq 10$, while the statistical calculation shows the increase of this ratio for primary fragments, as it was discussed above in the Introduction. Unfortunately, this effect seems to be completely washed out in the $\langle N/Z \rangle$ ratio versus Z dependence for *cold* fragments, Fig.6d.

The same secondary deexcitation procedure implemented in SMM (see Ref. [32]) was applied for the cooling of the hot fragments produced either dynamically or statistically. In the final products there is an universal decrease of the $\langle N/Z \rangle$ with Z , due to a larger Coulomb barrier for the emission of light charged particles by heavier hot fragments. That results in the increased relative contribution of the neutron emission with respect to the charge particle emission for the deexcitation of heavier hot fragments. The fact that all calculations produce the same dependence $\langle N/Z \rangle(Z)$ for cold fragments leads to the conclusion that the excess neutrons of hot fragments present in the SMF and SMM results with initial source $Z = 63$ (Fig. 6c, solid histogram and diamonds) are very weakly bound. They can then escape from the compound nucleus at the very first steps of the deexcitation process. This first-chance neutron emission almost does not change the excitation energy of the compound system. Therefore, the subsequent de-excitation steps proceed almost in the same way in all calculations. Of course in the evaporation chains we have now to insert nuclear structure properties of very exotic nuclear systems, which are largely unknown. So we can expect a quite large uncertainty in the predictions of the secondary deexcitation described using the method of Ref. [32] or any other sequential decay codes. Therefore we believe that the performed calculations can provide some guidelines for an experimental investigation of this phenomenon.

B. Dispersions

The difference between dynamical and statistical calculations is particularly pronounced in the dispersions of the N/Z ratio for each Z (Fig. 7). For hot fragments, the statistical calculations produce a factor of $2 \div 5$ larger dispersion even in the cases when there is no difference in the mean values of the N/Z (compare Fig. 6 a,b to Fig. 7 a,b). As we will see in the following, the variances are so large that the results presented below are mostly sensitive to that and not much depending on the mean values. Physically, this difference is related to a more deterministic way of the fragment formation in the SMF, that prohibits the strong deviations of the N/Z ratio from its mean value. Again, the subsequent deexcitation of the hot fragments seems to wash out completely all the differences in the cold IMFs (see Fig. 7d).

The previous discussion was mostly concentrated on the properties of hot primary fragments. We think it is possible to find some experimental observables which are sensitive to the differences between dynamical and statistical results for the hot fragments by looking at the products of their secondary decay. There is already an existing experimental technique based on a correlation function analysis that allows to attribute a secondary light charged particle to an IMF from which it was emitted [33].

In Fig. 8 we plot the yield ratios of ${}^4\text{He}$ to ${}^3\text{He}$, (a), and ${}^3\text{H}$ to ${}^3\text{He}$, (b), only emitted from the primary IMFs, as a function of the N/Z of the source. In this way we avoid the problem of preequilibrium particles and particles directly produced in the multifragment breakup. The dynamical calculation gives always larger ratios than the statistical one. The difference increases for the high asymmetric source ($A = 197$, $Z = 63$, $N/Z = 2.13$). This difference is due to a larger dispersion of the N/Z ratio for the hot SMM fragments. In the neutron excess region the production of a proton rich light particle becomes extremely sensitive to small changes of the N/Z of the primary fragments. Therefore, larger fluctuations of the N/Z ratio of hot fragments in the statistical calculation (see Fig. 7c) cause a dramatic enhancement of the ${}^3\text{He}$ production with respect to the dynamical calculation.

IV. CONCLUSIONS

We have performed a comparative study of the multifragmentation of highly excited asymmetric spherical sources within the dynamical and the statistical models. In spite of the general coincidence of the results, two clear differences in the isotopic composition of the hot primary fragments for a neutron rich initial source have been observed: (i) in the dynamical calculation the average N/Z ratio decreases with charge number $Z \geq 3$, while in the statistical one it increases; (ii) the dispersion of the N/Z ratio for a given charge number Z of hot fragment is much larger in the statistical calculation than in the dynamical one. Both effects seem to be largely reduced in the final fragments seen in the detectors. There is however a chance that some signatures of differences in isotopic content and excitation energy of primary fragments could survive. A good observable seems to be the isotopic ratio of light charged particles emitted from hot primary fragments.

We remark that, as already stressed in the Introduction, the point i), i.e. more symmetric primary fragments produced with the spinodal mechanism, is present for all effective interactions: the *magnitude* of the effect is sensitive to different behaviours of the symmetry term at *subnuclear* densities [13].

To disentangle between the two models a comparison of fragmentation data for some extremely neutron rich sources $N/Z \sim 2$ is required. A good possibility would be to look at the fragment produced in the midrapidity region in semiperipheral collisions of neutron excess nuclei: taking advance of the "neutron skin" effect we could study properties of fragments produced from a highly asymmetric interacting nuclear matter.

Some recent data on charge asymmetry effects on fragment production seem to be in a qualitative agreement with the signatures of the dynamical model, although a more precise analysis must be performed:

- 1) More neutron rich systems are producing more symmetric and less excited primary intermediate mass fragments [18,19,22];
- 2) Such effects are disappearing for central collisions above 100 $AMeV$ beam energy [22];

in the dynamical picture the expansion phase becomes too fast and the instability growing times cannot be matched;

3) Opposite behaviour is observed for light ions produced in the midrapidity region, that appear more neutron rich than the average N/Z of the composite system [17].

It should be mentioned here that the result 1) can be obtained also in recently developed thermodynamical models [10,34].

If all these signatures will be confirmed, from medium energy heavy ion collisions we will have a new powerful method to study the symmetry term of the nuclear Equation of State at subnuclear densities, of large interest for the structure of unstable nuclei as well as for astrophysics [35]

ACKNOWLEDGEMENTS

We are grateful to U. Mosel, W. Cassing and H. Lenske for fruitful discussions. Two of us (A.B.L.) and (A.S.B.) acknowledge the hospitality and support of INFN (LNS-Catania and Bologna) where the most part of this work was done, and one of us (A.B.L.) acknowledges the support of BMBF and GSI and the hospitality of the Institut für Theoretische Physik at the University of Giessen.

REFERENCES

- [1] J.P. Bondorf in "Multifragmentation" (Hirschegg 99) Ed.s H. Feldmeier, J. Knoll, W. Noerenberg and J. Wambach, GSI 1999, p.11;
I.N. Mishustin, Nucl.Phys. A **630** (1998) 111c and ref.s therein.
- [2] D.H. Gross, Phys.Rep. **279** (1997) 119 and ref.s therein.
- [3] A. Guarnera, M. Colonna and Ph. Chomaz, Phys. Lett. **B373** (1996) 267; M. Colonna, Nucl. Phys. A **630** (1998) 136c.
- [4] M. Colonna, M. Di Toro and A. Guarnera, Nucl. Phys. A **580** (1994) 312.
- [5] D. Durand, Nucl. Phys. A **630** (1998) 52c.
- [6] M.F. Rivet et al. (INDRA Collab.), Phys. Lett. B **430** (1998) 217 and in "Multifragmentation", see Ref.[1], p.293-305
- [7] R. Bougault et al. (INDRA Collab.), in "Multifragmentation", see Ref. [1], p.24-35.
- [8] G. Baym, H.A. Bethe and C.J. Pethick, Nucl. Phys. A **175** (1971) 225.
- [9] J. Konopka, H. Graf, H. Stöcker, and W. Greiner, Phys. Rev. C **50** (1994) 2085.
- [10] H. Müller and B.D. Serot, Phys. Rev. C **52** (1995) 2072.
- [11] Bao-An Li, C.M. Ko, Nucl. Phys. A **618** (1997) 498.
- [12] S. Ray, J. Shamanna, T.T.S. Kuo, Phys. Lett. B **392** (1997) 7.
- [13] M. Colonna, M. Di Toro, A.B. Larionov, Phys. Lett. B **428** (1998) 1.
- [14] V. Baran, M. Colonna, M. Di Toro and A.B. Larionov, Nucl. Phys. A **632** (1998) 287.
- [15] M. Colonna et al., in "Multifragmentation" see Ref. [1], p.322-327.
- [16] S.J. Yennello et al., Phys. Lett. B **321** (1994) 15.
- [17] J.F. Dempsey et al., Phys. Rev. C **54** (1996) 1710.

- [18] G.J. Kunde et al., Phys. Rev. Lett. **77** (1996) 2897.
- [19] G. Kortemeyer, W. Bauer and G.J. Kunde, Phys. Rev. C **55** (1997) 2730.
- [20] L.G. Sobotka et al., Phys. Rev. C **55** (1997) 2109, and in "Multifragmentation", see Ref. [1], p.72-81.
- [21] S. Yennello et al., in "Heavy Ion Physics", Ed.s Yu.Ts. Oganessian and R. Kalpakchieva, World.Sci.1998, p.253-260.
- [22] M.L. Miller et al., Phys. Rev. Lett. **82** (1999) 1399.
- [23] I. Bombaci, in "Perspective on Theoretical Nuclear Physics", ed. S. Rosati et al. (ETS-Pisa, 1996) p. 223.
- [24] M. Prakash et al., Phys. Rep. **280** (1997) 1.
- [25] A. Atalmi et al., Phys.Rev. C **58** (1998) 2238 and ref.s therein,
A. Bonasera et al., Phys.Rev.Lett. **78** (1997) 187
- [26] J.P. Bondorf, A.S. Botvina, A.S. Iljinov, I.N. Mishustin, K. Sneppen, Phys. Rep. **257** (1995) 133.
- [27] Chr. Jung, W. Cassing, U. Mosel, R.Y. Cusson, Nucl. Phys. A **477** (1988) 256.
- [28] M. Colonna, Ph. Chomaz and J. Randrup, Nucl. Phys. A **567** (1994) 637.
- [29] M. Colonna and Ph. Chomaz, Phys. Rev. C **49** (1994) 1908.
- [30] M. Colonna, N. Colonna, A. Bonasera and M. Di Toro, Nucl.Phys. A **541** (1992) 295.
- [31] J.P. Bondorf, A.S. Botvina, I.N. Mishustin and S.R. Souza, Phys. Rev. Lett. **73** (1994) 628.
- [32] A.S. Botvina, A.S. Iljinov, I.N. Mishustin, J.P. Bondorf, R. Donangelo and K. Sneppen, Nucl. Phys. A **475** (1987) 663.

- [33] N. Marie et al., Phys. Rev. C **58** (1998) 256.
- [34] Ph.Chomaz and F.Gulminelli, Nucl.Phys. A **647** (1999) 153.
- [35] "It is important to put the properties of *neutron* matter at *subnuclear* densities on as firm a footing as possible, not only for astrophysical applications, but also for interpreting terrestrial experiments with coming radioactive beam facilities" C.J. Pethick and D.G. Ravenhall, in "The lives of neutron stars", NATO ASI Series C, Vol.450, 1993.

FIGURE CAPTIONS

Fig. 1 Number density of hot fragments as a function of distance from the center of source with $Z = 63$ for the SMF calculation at the time step $t = 150$ fm/c. Solid, short- and long-dashed lines correspond to fragments with charge numbers $Z = 1 \div 2$, $3 \div 10$ and ≥ 11 respectively.

Fig. 2 Kinetic energy of a fragment as a function of the charge number for the source with $Z = 63$. Dashed (solid) histogram and stars (squares) show SMF and SMM results before (after) Coulomb acceleration.

Fig. 3 Charge yields of hot (a,b,c) and cold (d) fragments normalized on the number of fragments per event. Histogram and diamonds – SMF and SMM results respectively with source $Z = 95$ (a), 79 (b) , 63 (c,d).

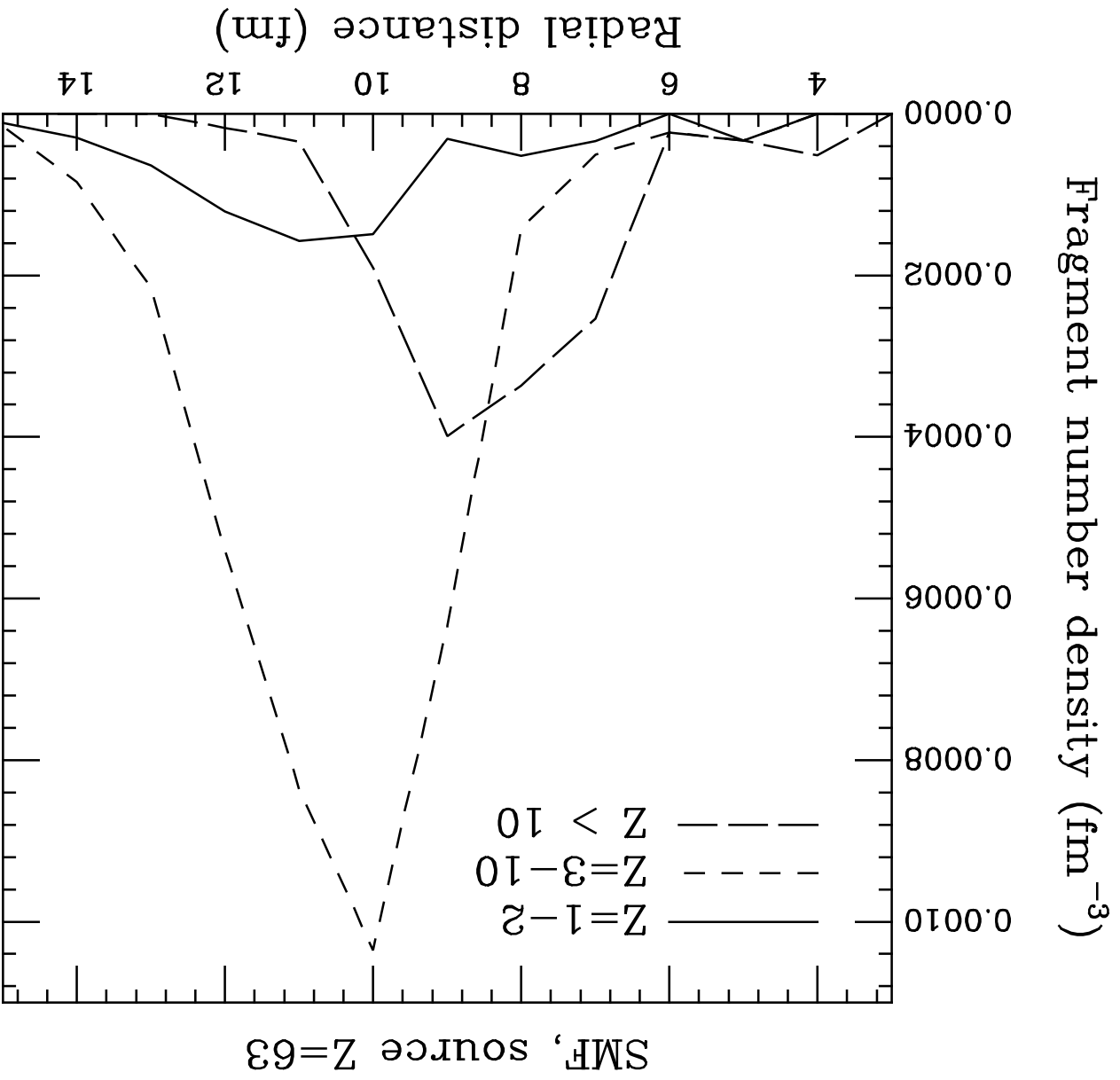
Fig. 4 IMF multiplicity distributions. Notations of curves and panels a,b,c,d like in Fig. 3.

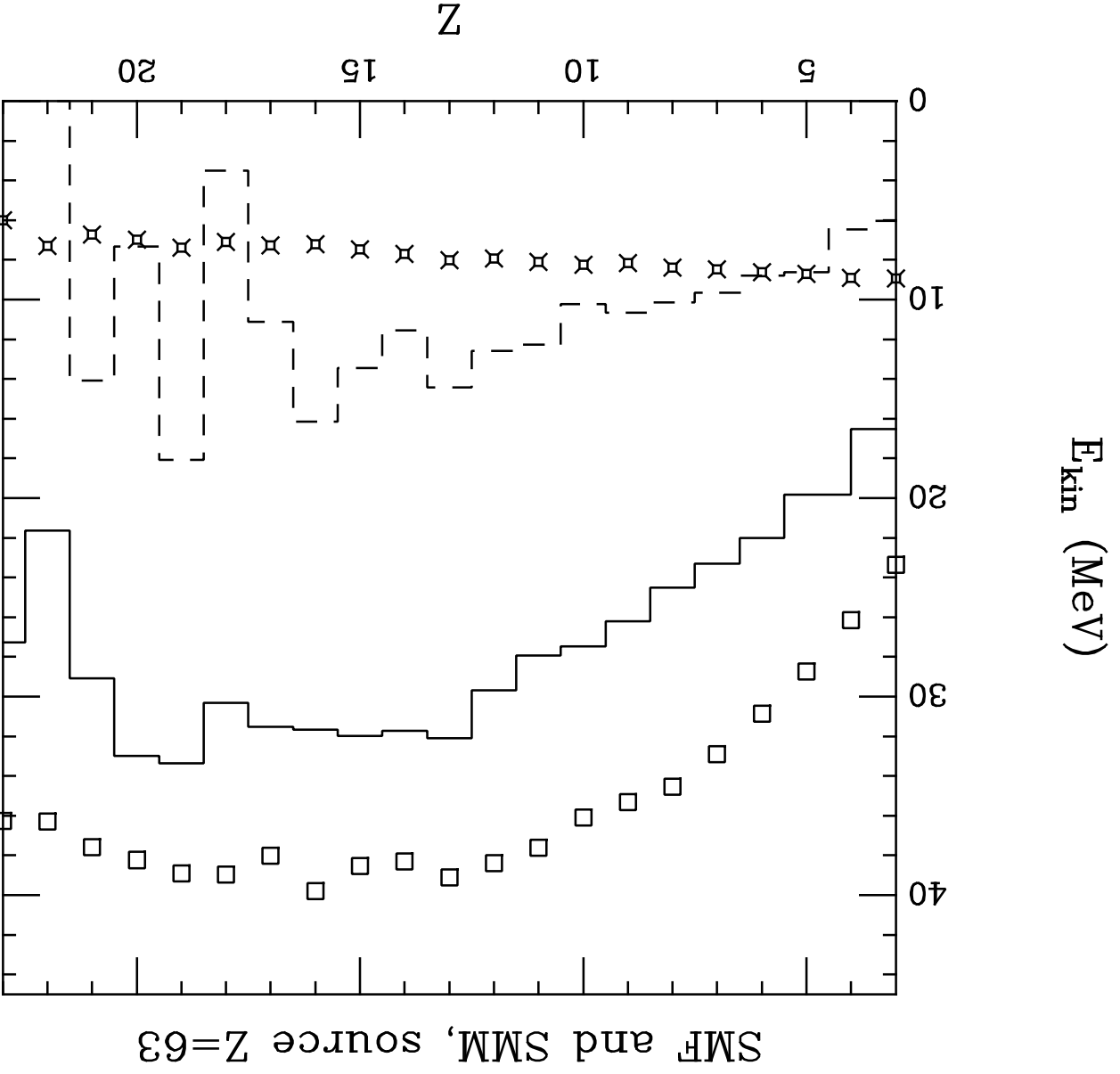
Fig. 5 Mean excitation energy per nucleon versus fragment proton number. Notations of curves and panels a,b,c like in Fig. 3.

Fig. 6 Mean neutron-to-proton ratio $\langle N/Z \rangle$ of fragments versus proton number Z . Notations of curves and panels a,b,c,d like in Fig. 3. Arrows show N/Z ratios of initial sources with $Z = 95$ (a), 79 (b) and 63 (c).

Fig. 7 Dispersion $\sigma_{N/Z} = \sqrt{\langle (N/Z - \langle N/Z \rangle)^2 \rangle}$ as a function of the fragment proton number Z . Notations of curves and panels a,b,c,d like in Fig. 3.

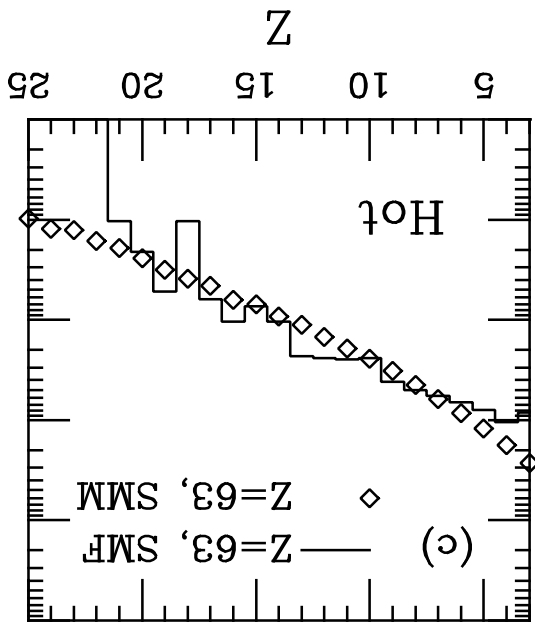
Fig. 8 Isotopic ratios ${}^4\text{He}/{}^3\text{He}$ (a) and ${}^3\text{H}/{}^3\text{He}$ (b) are plotted as a function of the N/Z of the source. Solid lines with errorbars show the SMF result (errors are statistical ones). Diamonds represent the SMM calculation.





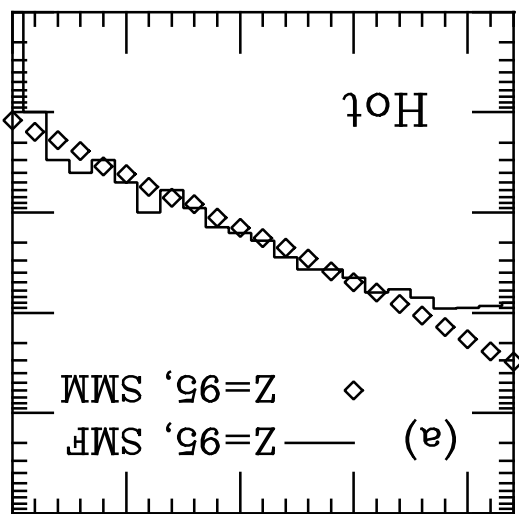
$Y(Z)$

10^{-3}
 10^{-2}
 10^{-1}
100
 10^1
 10^2

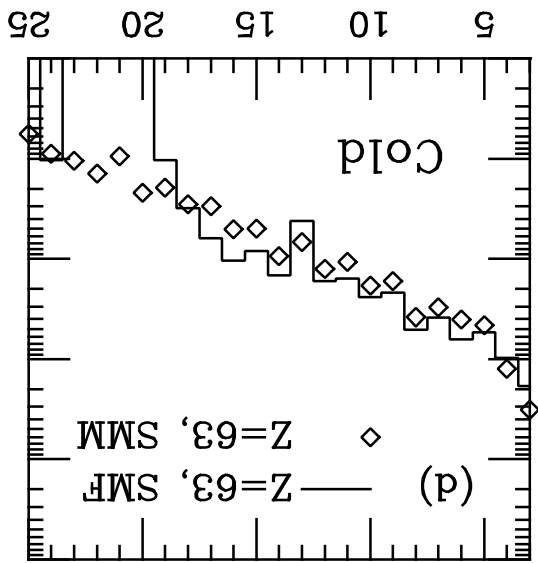


$Y(Z)$

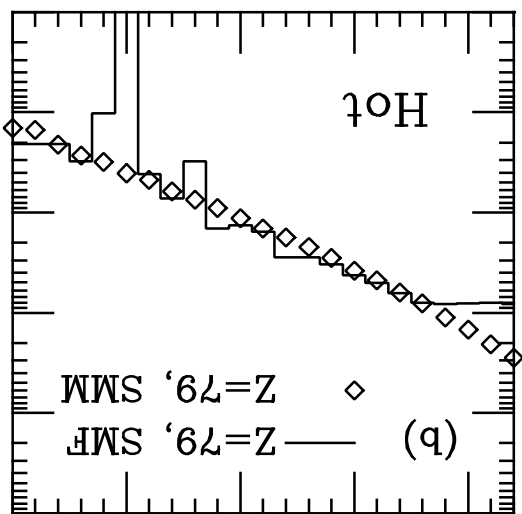
10^{-3}
 10^{-2}
 10^{-1}
100
 10^1
 10^2



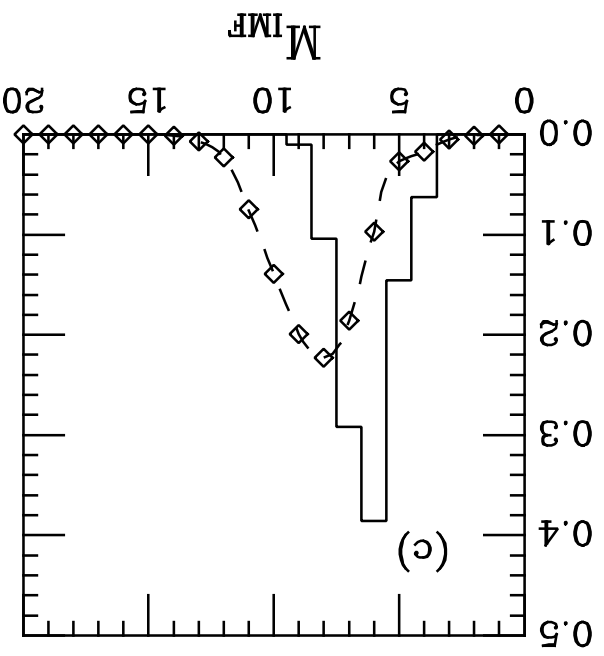
Z



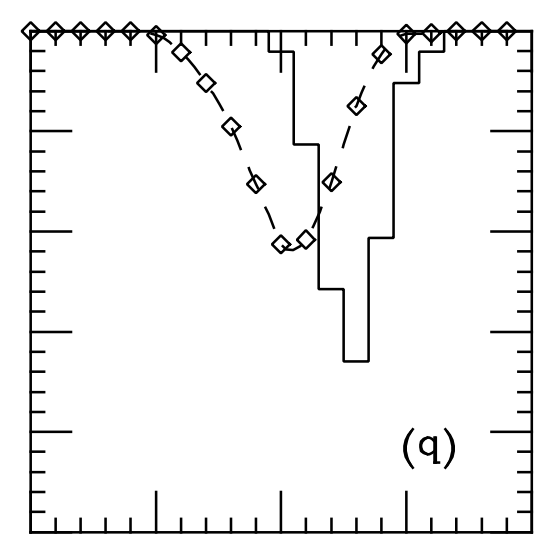
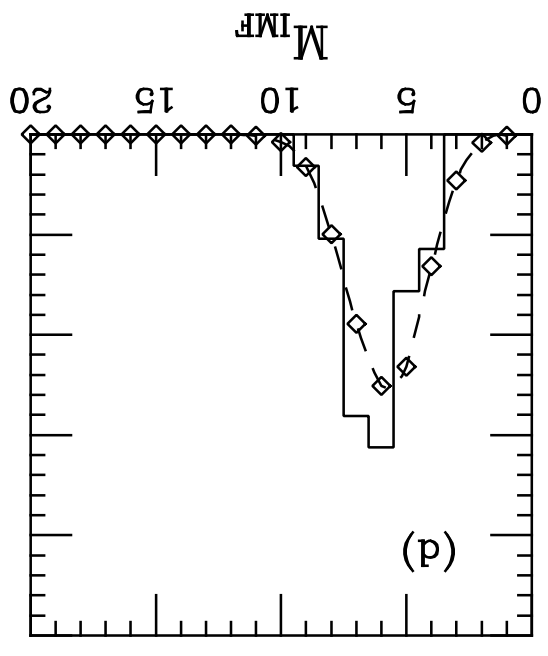
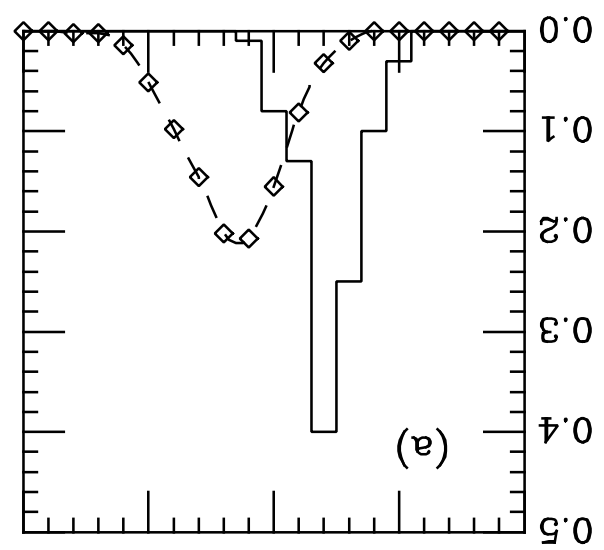
Hot



$P(M_{IMF})$



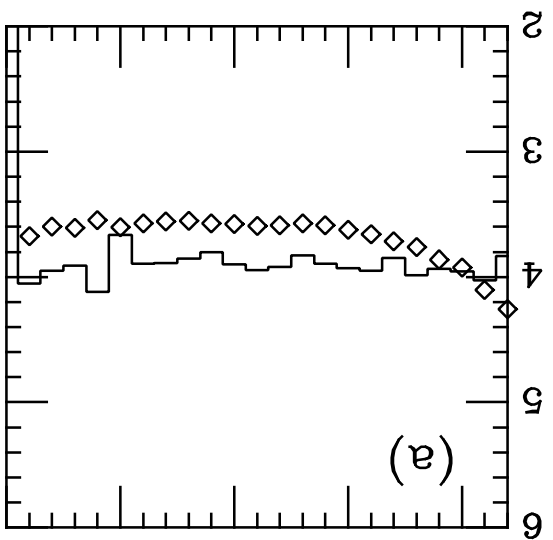
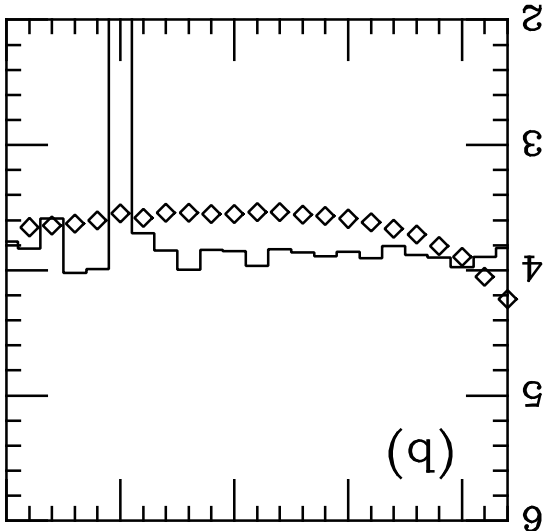
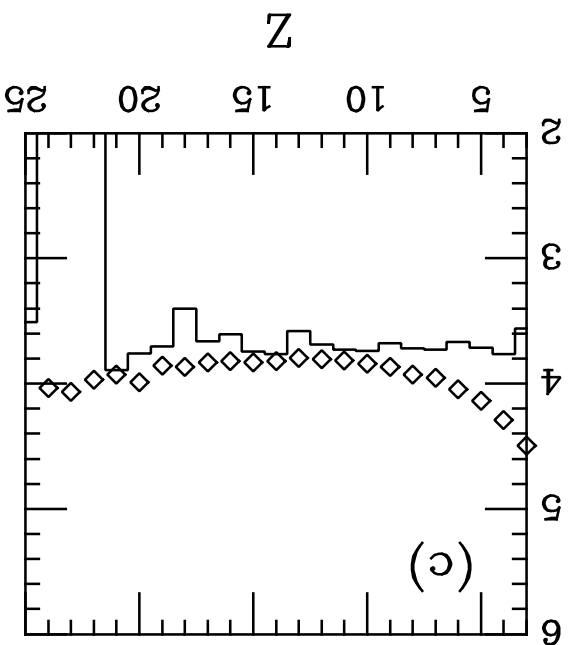
$P(M_{IMF})$



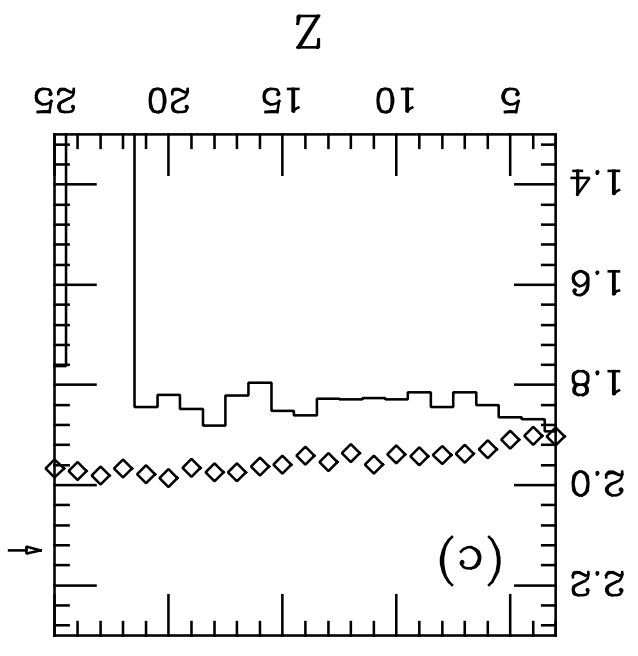
E_{exc} (MeV/nucleon)

E_{exc} (MeV/nucleon)

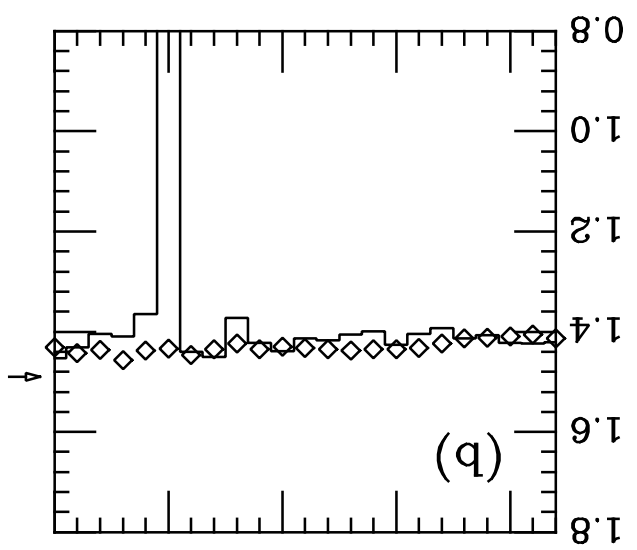
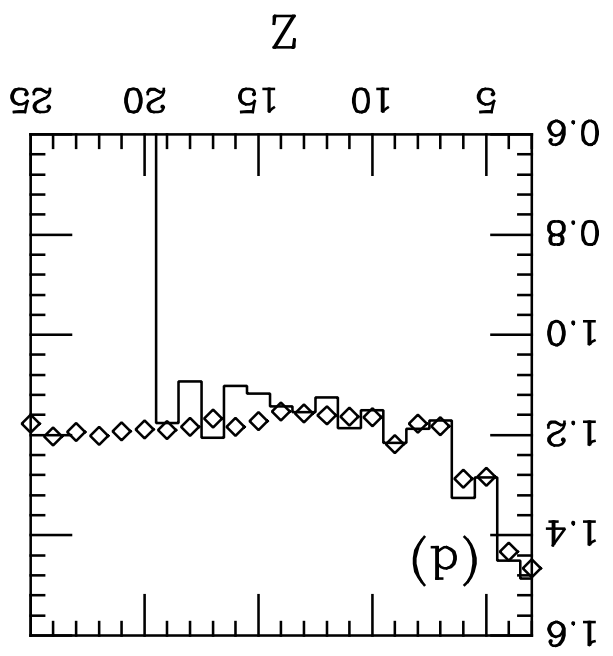
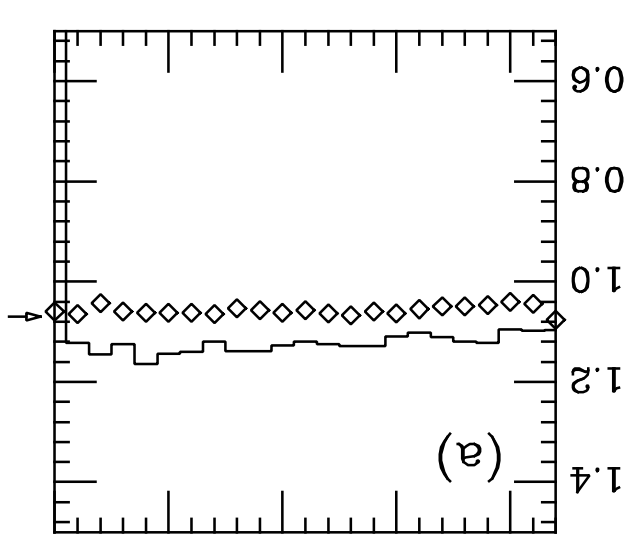
E_{exc} (MeV/nucleon)



$\langle N/Z \rangle$

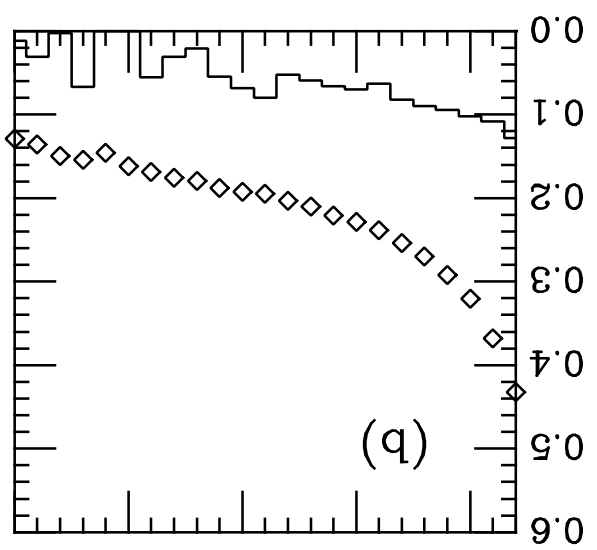
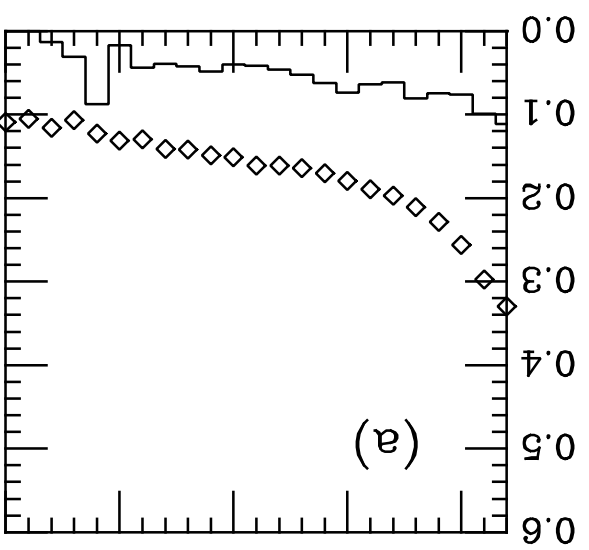
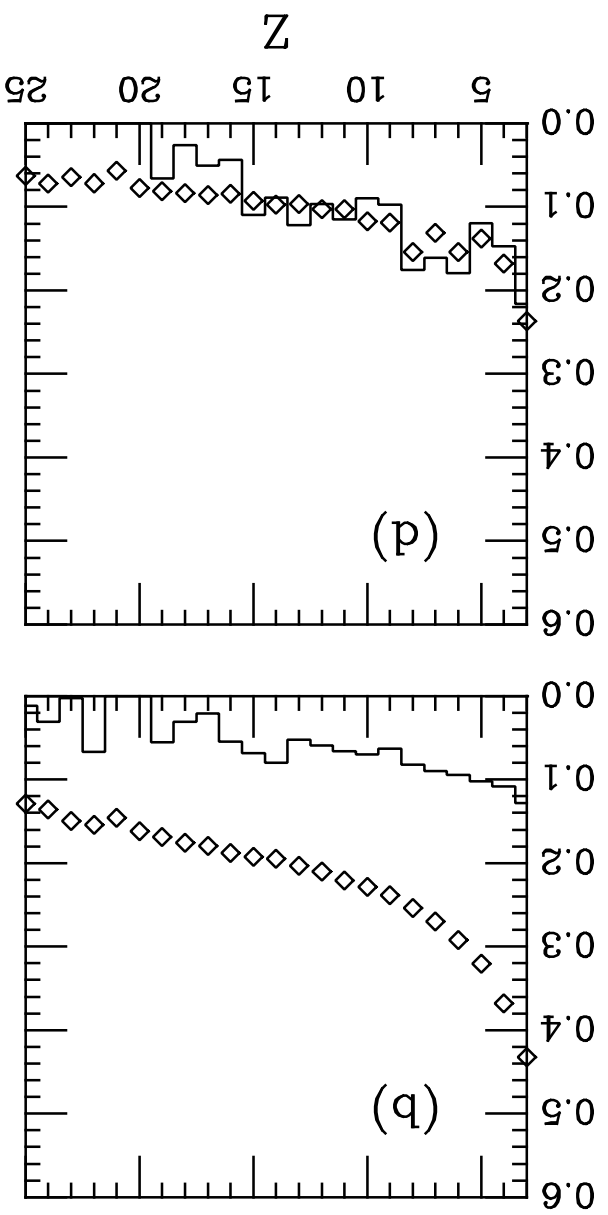
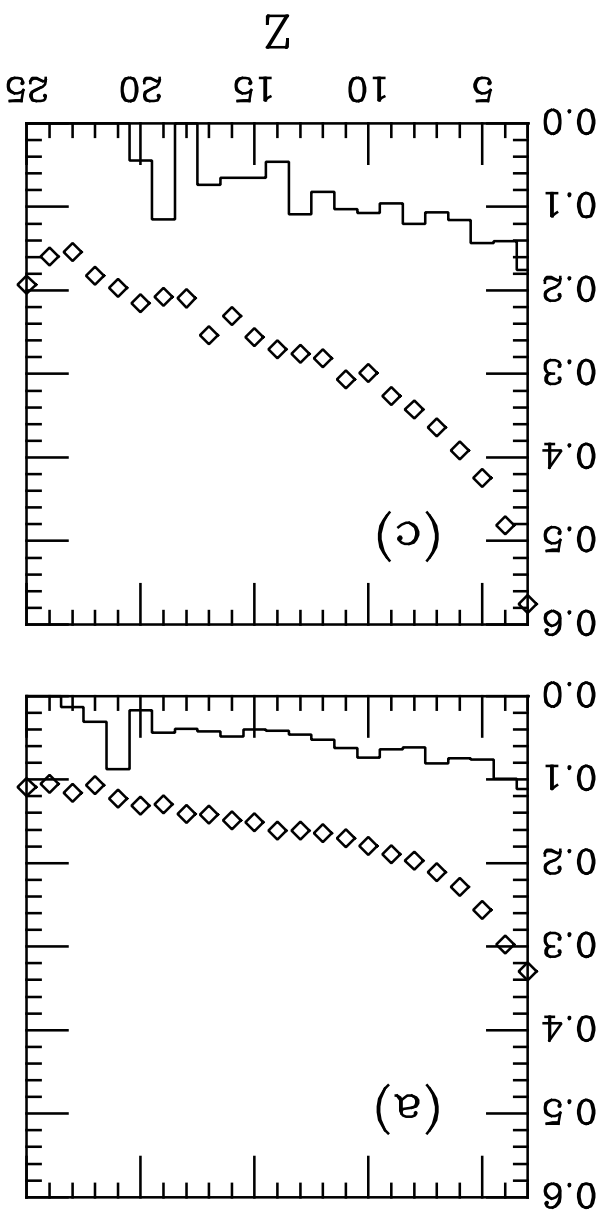


$\langle N/Z \rangle$

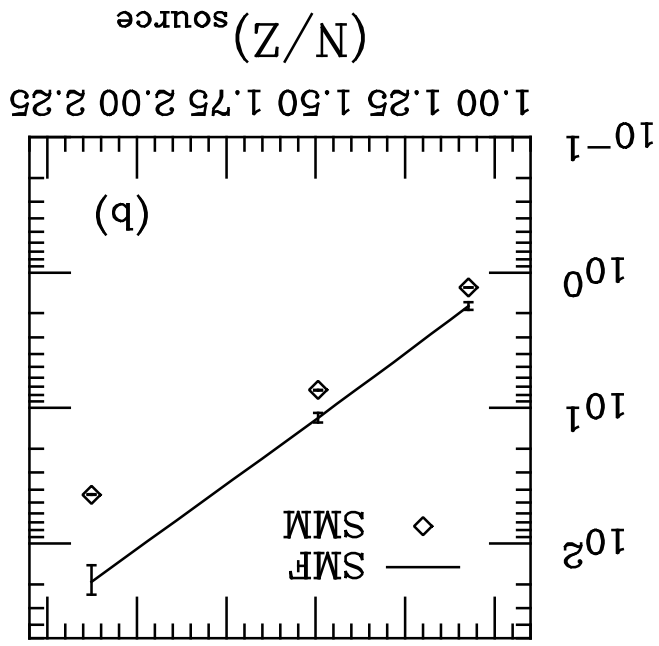


Dispersion of N/Z

Dispersion of N/Z



${}^3\text{H}/{}^3\text{He}$



${}^4\text{He}/{}^3\text{He}$

